JOURNAL OF MATERIALS SCIENCE 27 (1992) 1989–2006

Review
Modelling and experimental studies of properties of TiN coatings

S. CHATTERJEE
Western New England College, Springfield, MA 01119, USA
T. S. SUDARSHAN
Materials Modification Inc., 2929-P1 Eskridge Center, Fairfax, VA 22031, USA
S. CHANDRASHEKHAR
AT&T Bell Laboratories, Holmdel, NJ 07728, USA

This paper reviews pertinent research in the area of theoretical modelling and experimental studies of the various properties of titanium nitride coatings. A brief description of methods commonly used for the deposition of TiN coatings is discussed first. The important properties of these coatings are presented next. Various theoretical models for hardness, adhesion and residual stresses, and experimental work, both in support of these models and on other relevant properties such as corrosion, abrasion and colour, are cited and discussed. Finally, research issues and developmental needs in pertinent areas are identified and explicated.

1. Introduction

The use of coatings for various purposes is an established technology. Coatings are utilized, for example, for decorative purposes, to enhance tribological properties of components, and to increase resistance to failure of cutting tools [1]. The titanium nitride (TiN) coating is a thin film deposited on an appropriate base, known as the substrate. Significant research, development and application of coatings has been evidenced in the last two decades. Some of the more important coating types are TiN, titanium carbide (TiC), hafnium nitride and carbide (HfN, HfC), titanium carbonitride (TiCN), aluminium oxide (Al_2O_3) etc. Of these coatings, TiN has a low coefficient of friction, high hardness, resistance to high temperature, and good adhesion to the substrate [2–4]. TiC coatings, developed in 1969 [1], possess high flank wear resistance while ceramic coatings are characterized by resistance to high temperature, chemical inertness, and resistance to flank and crater wear.

The objective of this paper is to present a review of the salient properties of TiN coatings and the techniques used to measure these properties. TiN is the dominant coating in use among all coating types, not only due to its excellent performance in increasing material removal rates but also because of its pleasing golden colour and resistance to wear and corrosion.

This paper is organized as follows. A brief description of methods commonly used for the deposition of TiN coatings is given first. The important properties of TiN coatings are discussed next. Various models and experimental research on hardness, adhesion, residual stresses, corrosion, abrasion, erosion and colour properties are reviewed thereafter. Finally, research issues and developmental needs in pertinent areas are identified and explicated.

1.1. TiN deposition methods

Various surface treatment methods such as nitriding, electroplating, chemical vapour deposition (CVD) and physical vapour deposition (PVD) are available for depositing coatings on components. Of these, CVD and PVD techniques are the predominant methods.

The CVD processes are characterized by high deposition temperatures and are used for depositing TiN films on carbide or ceramic substrates. Typical CVD process parameters are [5]: (i) temperature (greater than 800 °C and typically up to 2000 °C; (ii) pressures (less than 1 atm and as low at 10^{-6} torr); (iii) precursors – these include reactive gases such as metal halides and carbonyls; reducing gases such as H_2; inert gases such as Ar; N_2; and other gases such as CH_4, CO_2, NH_3 and other hydrocarbons.

In CVD a chemical reaction occurring between a titanium compound and reactive gases leads to the formation and deposition of TiN on substrates in a closed reactor. Plasma-assisted CVD (PACVD) and laser-assisted CVD (LACVD) are variations of this technique [5].

In direct contrast to the CVD techniques, PVD techniques require a relatively low coating temperature (approximately 500 °C or less). The primary PVD processes are evaporation, sputtering and ion-plating. In the evaporation process, the condensation of the target material vapour on a substrate produces the thin film. This type of evaporation process suffers from drawbacks [6]. First, non-stoichiometric films

0022–2461

can result due to partial dissociation of compounds. Second, for high melting-point compounds a high power density is required to obtain appreciable and economical evaporation rates, leading to operational problems with the source for extended run periods. In sputtering, ions of the target are liberated by bombardment by inert gas ions and attracted to the workpiece. Thus, to deposit Ti, a Ti target would be bombarded and the resulting Ti ions deposited on a substrate in a vacuum chamber. Various modifications of this process are used to enhance the yield rate. In magnetron sputtering (MS) magnets are used to confine a small target area for material removal. A large substrate area can thus be deposited and the deposition rate is also quicker [7–9]. Sputter ion plating (SIP) is another variation of the sputtering process, and in SIP d.c. and r.f. magnetron devices with substrate biasing enable high deposition rates to be achieved [10, 11].

The ion plating (IP) process deposits an initially molten target material on to a pre-heated substrate. The substrate is pre-heated by ion bombardment to raise it to the required deposition temperature [12]. Melting of the target is accomplished by an electron-beam gun. Various modifications of the IP technique include, among others, activated reactive ion plating (ARIP) [13] and cathodic arc plasma deposition [CAPD] [14].

In summary, the two major deposition methods are CVD and PVD. Modifications of the CVD method include PACVD and LACVD. For the PVD technique evaporation, sputtering and ion plating constitute the three main classes.

2. Salient properties of TiN coatings

The most important properties of TiN coatings to be discussed in this paper can be divided into two categories: (i) mechanical properties and (ii) metallurgical properties. Some of the major mechanical properties are: (a) yield strength, (b) ultimate tensile strength, (c) transverse rupture strength, (d) hardness, (e) adhesion, (f) wear and corrosion resistance. For thin TiN films, hardness and adhesion are the two most widely considered properties because these properties are relatively surface-specific and mostly govern the quality of the film. The metallurgical properties include microstructure, grain size and grain boundary structure, and texture and orientation. In this paper, the mechanical properties, (a)–(f), of TiN coatings and colour properties will be discussed.

Uniaxial tension testing of TiN films provides data regarding Young's modulus, yield strength, ultimate tensile strength, work hardening rate and ductility of these films [15]. It should be noted here that specimens for tensile testing are thin TiN films which may be made by electrical discharge machining of thicker films, or by dissolution of substrate by appropriate medium (15).

Young's moduli of sputtered TiN films on steel have been determined using flexural resonance of the composite [16]. The sample flexural resonance frequency is related to the Young's modulus and sample dimensions and, therefore, the Young's modulus can be determined by determining the resonance frequency of a sample of known dimensions.

Biaxial tension testing is also done on thin films stripped mechanically or by dissolution from the substrate [15]. This yields the biaxial stress and strain at the centre of the film. For both tensile and bulge testing, the results or their interpretation should not be affected by film edge effects, because loading effects on film edges are likely to be different from the centre resulting in different values of the parameter at the edges.

For thin TiN films, microhardness testing is the most commonly used method and conventional Vickers and Knoop microhardness tests can be applied. However, the indentation depths should not be more than 10% of the film thickness for true hardness measurements, otherwise substrate hardness effects mask the true hardness values [17]. This necessitates substantially reduced indentation loads. However, at very low loads (less than 100 g) hardness of films is seen to be dependent on applied load and significant errors in hardness value may result. This has led to the development of ultra-low load indentation hardness testers for measuring elastic modulus and hardness of films [18] and of theoretical hardness measurement models. These models and their correlations with experimentally obtained hardness measurements will be discussed in a later section.

Adhesion of films is determined by the well-known scratch testing method. In this process, a 120° loaded diamond stylus is repeatedly drawn across the sample. The load on the stylus is increased with each passage until the coating is stripped completely from the surface. This film stripping load is termed the critical load (L_c) and is a measure of film adhesion.

Wear and corrosion resistance of TiN films are measured by subjecting the films to abrading particles (sand, glass, etc.) for wear resistance testing or exposing them to a corrosive environment (acids, saline water, etc.) for corrosion resistance testing.

One reason for the widespread acceptance of TiN coatings is their pleasing golden colour. A measure of the quality of this property is determined by the luminance, redness and yellowness of the films. The processing parameters have been found to affect the colour of the film; this and other aspects are discussed later.

In summary, this section has reviewed the salient mechanical properties of TiN coatings. These properties play a significant role in determining the final quality of the film for a given application. Theoretical and experimental work on these properties are studied next.

2.1. Strength properties of TiN films

As mentioned before, tensile testing is performed on TiN films to determine strength properties such as the Young's modulus, Poisson's ratio, the biaxial modulus, the flexural modulus and the torsional modulus. Experimentally, an ultra-low load hardness tester is used to record load–displacement characteristics of a

film. Some of the strength properties may be estimated from a typical plot, such as that shown in Fig. 1, in which indentation depths are noted during both loading and unloading cycles.

Results from flexural resonance frequency testing of TiN samples by Torok *et al.* [16] indicate that the modulus increased steadily with N_2 level of reactive gas to a maximum at stoichiometric composition. This effect is shown in Fig. 2. These authors also compared the resulting modulus with these of ZrN, HfN, and TiN from other research. These comparisons are also shown in Fig. 2.

3. Hardness studies of thin films

3.1. Theoretical modelling of thin-film hardness

Jonsson and Hogmark [19] developed a simple model for the measurement of microhardness of thin films.

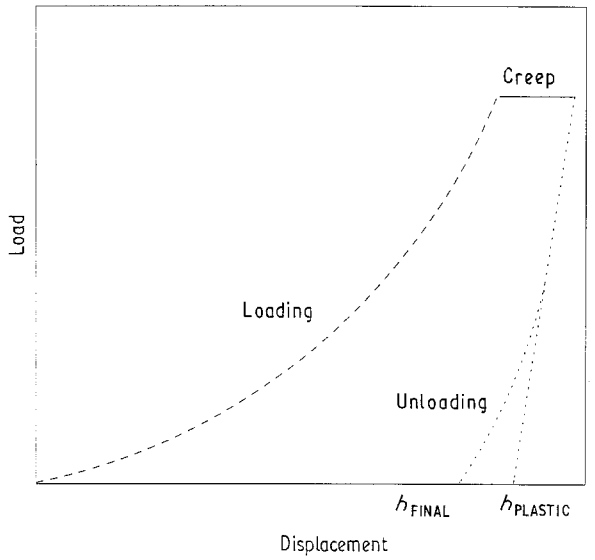

Figure 1 Typical load–displacement curve obtained using an ultramicrohardness instrument showing the difference between the plastic and final depths (adapted from Hardwick [15]).

Their model utilized idealized deformation geometries of a thin film subjected to indentation load as shown in Fig. 3. From the area A_f of deformed film and area A_s of deformed substrate the composite hardness H_c was expressed as

$$H_c = \frac{A_f}{A}H_f + \frac{A_s}{A}H_s$$

where $A = A_f + A_s$, H_f is the film hardness and H_s is the substrate hardness. Given a film thickness, this model was able to compute film hardness after recording the composite hardness.

The model was tested for chromium films deposited on hard and soft substrates. The measured values indicated validity of the model for soft substrates. No other film material hardness was evaluated by this model. However, the model failed to predict the hardness accurately for indentation depths less than the thickness of the film.

It has been found that TiN film hardness is dependent on load at small indentation sizes [20]. This is known as the indentation size effect (ISE) [17, 21]. In the microhardness regime (loads less than 1 kg) the hardness expression is

$$H = qd^{m-2}$$

where H is the hardness, q is a constant, m is the ISE index and d is the indentation depth. For $m > 2$, hardness decreases with decrease in indentation size; for $m < 2$ hardness increases with decrease in indentation size while for $m = 2$ there is no ISE.

The ISE concept has been incorporated in hardness prediction models [21, 22]. From studies of thin film indentation, it has been postulated that the morphology of the plastically deformed zone beneath the indenter will depend on the film–substrate combination. The expected plastic zone morphology is shown in Fig. 4 for films harder and softer than their substrates. Thus, for softer substrates and harder films and vice versa, deformation of substrate is modified at the interface.

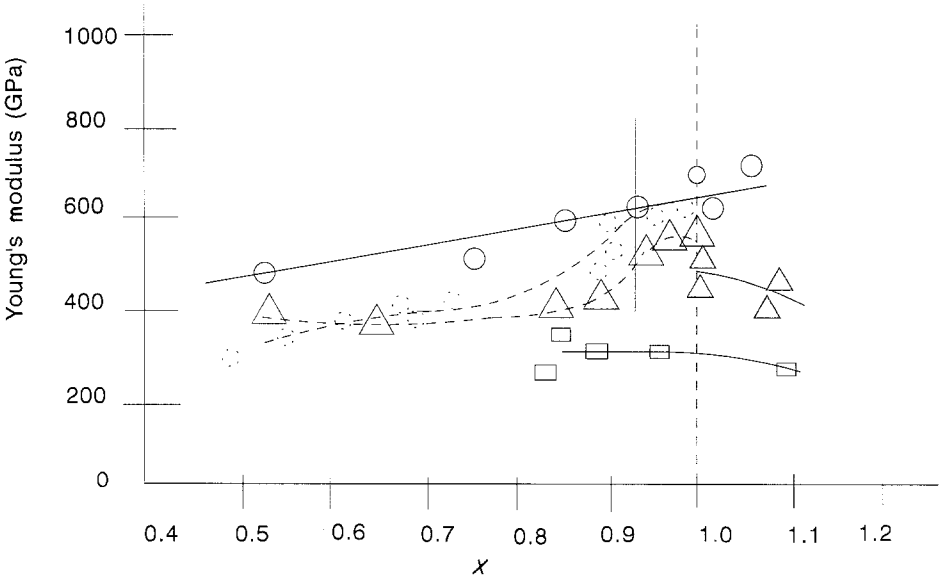

Figure 2 Young's modulus data as a function of nitrogen content: X = nitrogen to metal ratio in MN_x (adapted from Torok *et al.* [16]). TiN: (○) Torok *et al.*, (○) Torok *et al.* CVD,( ) Comparison data. ZrN: (△) Torok *et al.*, (Δ) Comparison data. HfN: (□) Torok *et al.*

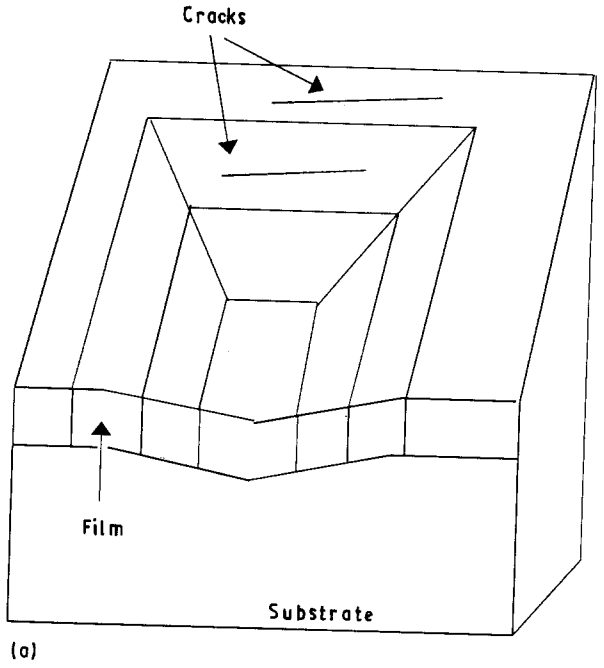

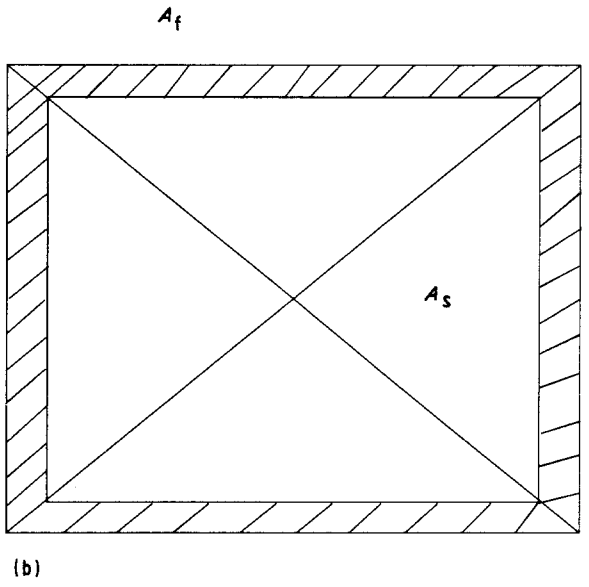

Figure 3 (a) Cross-section of an indentation on a coated material; (b) load-supporting areas A_f and A_s of the film and the substrate, respectively (adapted from Jonsson and Hogmark [19]).

From this deformation morphology the expression for computing the film hardness H_f from the composite hardness H_c and substrate hardness H_s is

$$H_c = \frac{V_f}{V}H_f + \frac{V_s}{V}\chi^3 H_s \quad \text{for } H_s < H_f$$

$$H_c = \frac{V_s}{V}H_s + \frac{V_f}{V}\chi^3 H_f \quad \text{for } H_f < H_s$$

where V_s and V_f are deforming film and substrate volume and $V = V_s + V_f$. The parameter χ is a factor by which the plastic zone radius changes. The volumes V_s and V_f can be calculated from the knowledge of indentation semi-diagonal length, the plastic zone radius and the indenter semi-angle.

3.2. Experimental studies of thin-film hardness

The validity of the above ISE model has been tested

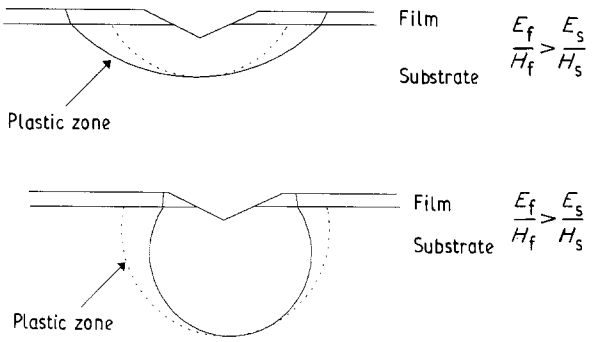

Figure 4 The expected modification to the plastic zone morphology when a rigid interface (strong adhesion) is present (adapted from Burnett and Rickerby [17]).

by microhardness measurements for TiN and WTiC deposited on metallic and non-metallic substrates. A fairly good agreement is seen between results obtained by this model and the Jonsson and Hogmark model [19] modified by ISE. The best results were obtained for $\chi = 1$. Fig. 5 shows the hardness dependence on indentation depth for TiN on tool steel. A reasonably good fit of hardness data was observed for TiN and WTiC on other substrates. A notable observation from hardness measurements is the difference in film hardness values between the surface and cross-section. Burnett and Rickerby [22, 23] attributed this to the microstructure and crystallographic anisotropy of the films. It should be noted here that the origin of ISE is not fully understood and experimental work has only been able to establish minimum film thicknesses necessary to avoid such ISE effect in a few cases [24].

The flow geometry of displaced substrate is influenced by the substrate–film combination [25]. For softer substrates a high amount of coating deformation may occur through pile-ups of material around the indenter to accommodate larger substrate deformation. Conversely, for harder substrates this pile-up may be much less. Thus, the modulus-to-yield stress ratio for substrate may be an important parameter for coating–substrate compatibility.

Indentation (Vickers hardness) and scratch tests were conducted by Knight *et al.* [25] to determine the substrate flow response. M42 and M2 tool steels, low-alloy steels and 18:8 austenitic steels were deposited with arc-evaporated TiN coatings. The hardness tests showed ISE effects at low loads. Fig. 6 shows such ISE effects at various loads. For softer substrates, a pile-up of material around the indenter was noted. The indentation evolved nested racks parallel to the edge of the indenter within the indentation; this effect was more pronounced for softer substrates. For harder substrates, cracking occurred in the substrate at increased loads. Cracks were either parallel to the interface or propagated into the substrate. The scratch test results indicated a decrease in critical load with increasing substrate hardness and an anomalous result for indenter penetration depths at hardness between 800 and 1400 H_V. It was seen that penetration depths for the material–coating combinations tested were much higher in this hardness range than expected. No plausible hypothesis is known for this; thus it is necessary to investigate the hardness/penetration depth and

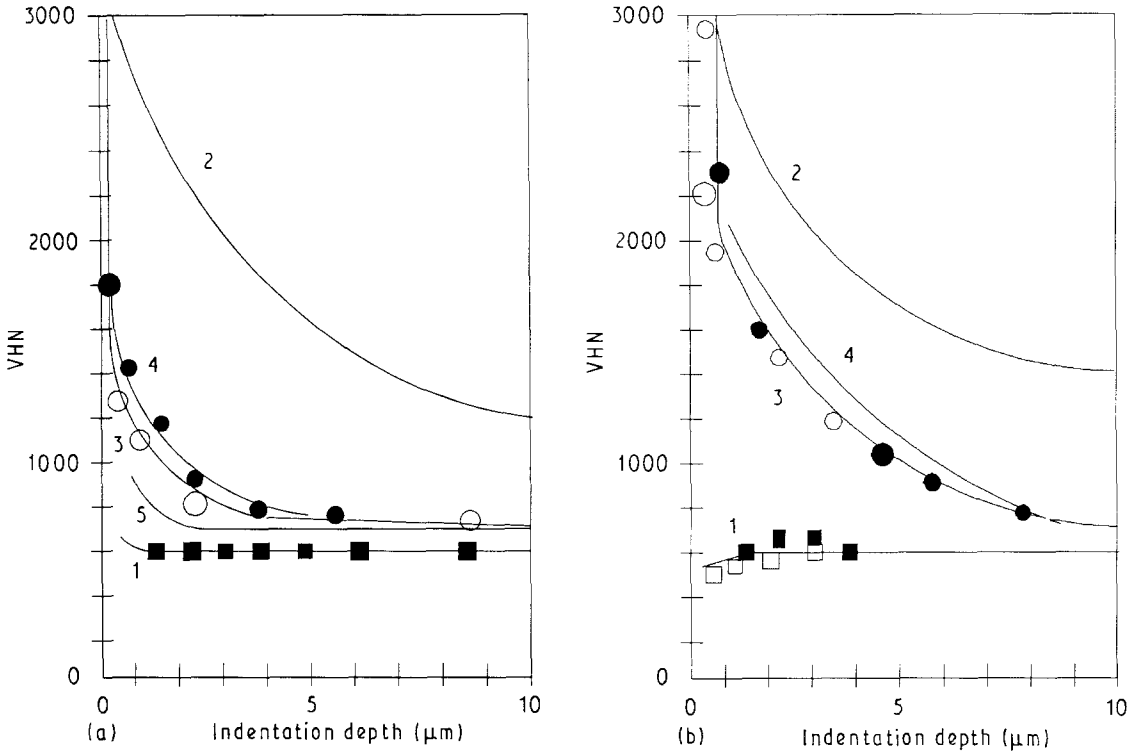

Figure 5 The hardness behaviour of TiN-coated tool steel (M2) (●, ○) for coatings (a) 25 μm thick, (b) 9 μm thick. The substrate hardness data (■, □) are also shown. Curve 1 is the substrate behaviour and curve 2 is the "bulk" hardness using the Burnett and Rickerby hardness model (curve 3), the Jonsson and Hogmark model incorporating ISE (curve 4), and the Jonsson and Hogmark model without ISE (curve 5). (Adapted from Burnett and Rickerby [22].)

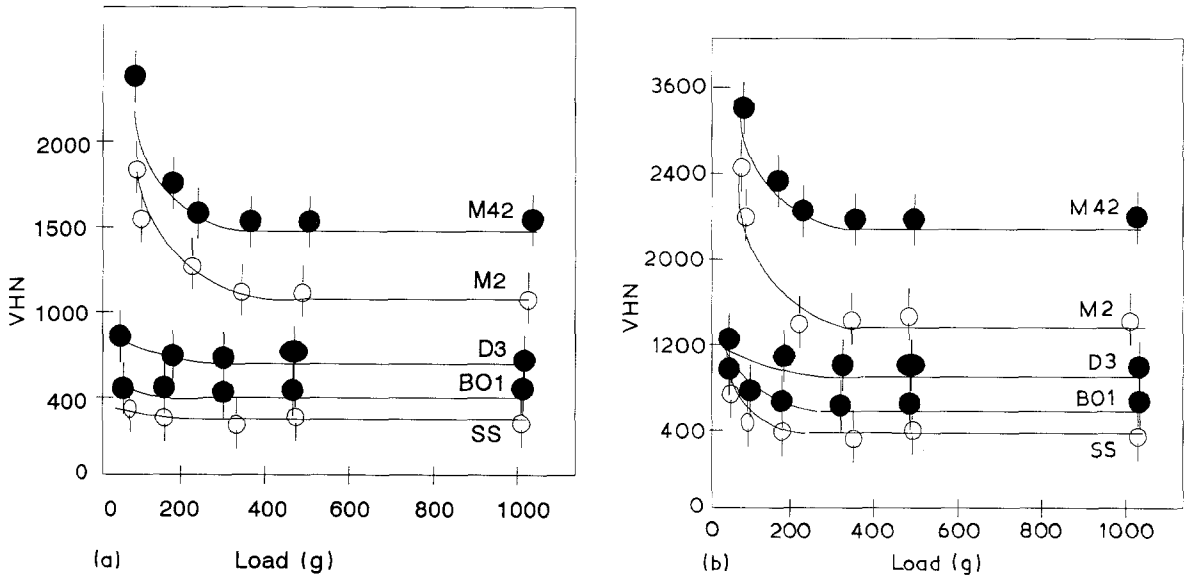

Figure 6 The load dependence of the Vickers microhardness of (a) the bare substrates with the coating polished away and (b) the coated substrates. Comparison of the figures shows the enhancement of hardness provided by the coating at low loads. (M42, M2) tool steels, (B01) low-alloy tool steel, (D3) chromium steel, (SS) stainless steel. (Adapted from Knight *et al.* [25].)

load dependence for TiN films on different substrates with respect to stress transmission through the coating, the interface conditions, or the substrate deformation response for this behaviour.

The substrate temperature dependence of the hardness of coatings is another important thin-film characteristic [26] and is shown in Fig. 7. It has been observed that coating hardness increases with temperature, due to a reduction in the film defect content. However, it has also been observed by other researchers that the hardness of TiN films tends to decrease with increased deposition temperature for both PVD and CVD. One possible explanation is the high-temperature oxidation of TiN resulting in a degrading effect on the film hardness.

A similar temperature dependence of microhardness was observed by Quinto *et al.* [27] for a series of TiN films deposited by both PVD and CVD methods. All films experienced a decrease in hardness with temperature with convergence of hardness, as seen in Fig. 8. Such decreases in microhardness are attributed to the release of stored elastic energy within the

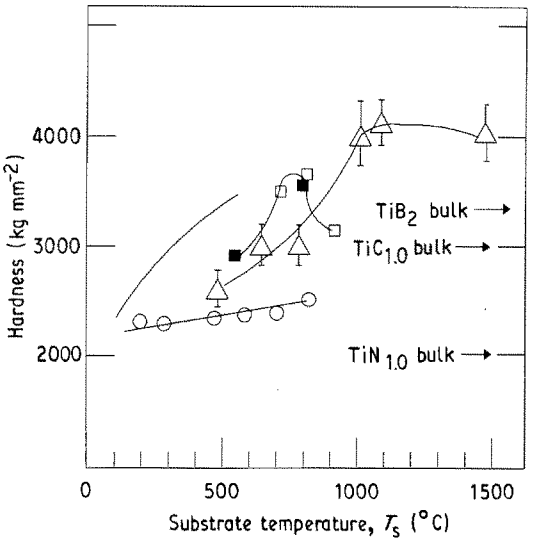

Figure 7 Film hardness as a function of substrate temperature for some refractory compounds: (○, —) TiN, (△) TiC, (□) TiB_2. Also shown are the corresponding bulk values. (Adapted from Sundgren and Hentzel [24].)

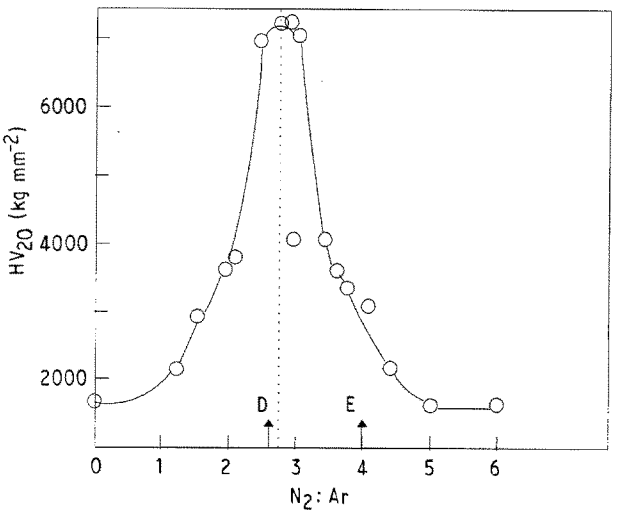

Figure 9 Microhardness of TiN layers deposited over a period of 20 min as a function of the nitrogen-to-argon flow rate ratio N_2: Ar. D and E represent variable deposition times for two sample sets. (Adapted from Valvoda *et al.* [28, 29].)

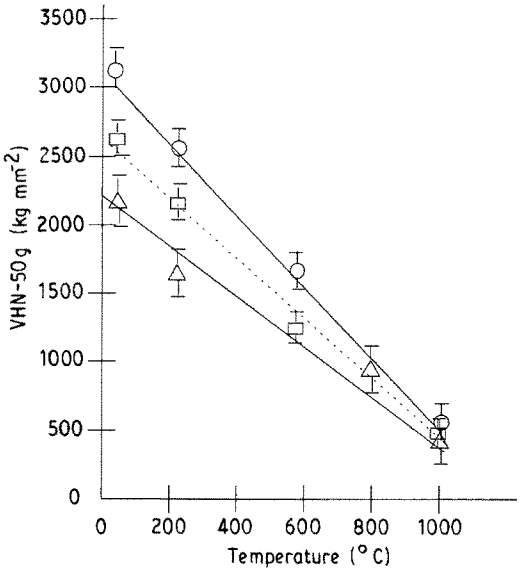

Figure 8 High-temperature VHN plots for coatings of (△, —) TiN, (□,---) ZrN and (○, —) HfN prepared by PVDMS (adapted from Quinto *et al.* [27]).

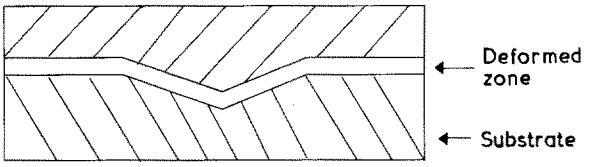

Figure 10 Actual shape of deformed plastic zone (adapted from Page and Knight [26]).

coating at higher temperatures, and are higher for PVD coatings than for their CVD counterparts.

The effect of coating thickness on microhardness has been investigated by Valvoda *et al.* [28, 29] and reveals a hardness dependence on coating thickness. Decreases in hardness values with decreases in thickness can be likened to the ISE effect of substrate discussed earlier. The researchers found evidence of an effect of the nitrogen content of reactive gas on the hardness of films, and attributed this to differences in phase microstructure [30] at different nitrogen contents. Fig. 9 shows such effects.

Conflicting reasonings relating hardness to microstructure have been offered by researchers. Wendler [31] observed an increase in hardness with annealing for films deposited by the activated reactive evaporation process. He suggested the increase in hardness to be due to the formation of a stable δ-TiN phase at the higher annealing temperature. Valvoda *et al.* [32], on the other hand, observed a decrease in microhardness of magnetron-sputtered TiN films with annealing due to release of strains and formation of ε-Ti_2N phase. Hibbs *et al.* [33] determined that the hardness of sputtered films with a single TiN phase was higher than that of magnetron-sputtered single-phase TiN film. Thus, it is seen that film properties depend on the evolved microstructure which in turn is dependent on the deposition process.

A survey of the literature revealed several interesting comparisons. The Burnett and Rickerby [21] hardness prediction model assumes the shape of the deformed plastic zone to be given by the shape in Fig. 4. However, the actual shape, as observed in reality, conforms to Fig. 10. Thus, the plastic zone morphology should be modified accordingly in hardness prediction models and the origin of ISE should also be investigated. It has also been noted that polishing of coatings results in coating loss which is not representative of the original composite [25]. In such cases, it is necessary to appropriately scale coating hardness values such that an accurate prediction of contact-induced hardness values may be possible because in reality, coatings are applied widely in rolling and abrasive contact applications. It is also necessary to investigate the inverse dependence of penetration resistance of TiN coatings at certain load ranges [25]. It seems that a decision support system for hardness prediction for various film–substrate combinations may be a useful tool and a valuable source of collective information on film properties and behaviour.

4. Adhesion studies of thin films

4.1. Theoretical modelling of thin-film adhesion

Adhesion is an extremely important property of thin films. The scratch testing method (schematically shown in Fig. 11) is a very widely used method for determining adhesion of films and adhesion predictor models have also been developed. In this section, models for adhesion prediction will be discussed and experimental work in scratch testing reviewed.

The energy balance approach may be used in determining adhesion of coatings in the scratch test [35]. This approach postulates that the energy stored in the coating is responsible for generating new surfaces at the original interface. The stored elastic energy in a length Δx of coating ahead of the indenter is expressed as

$$\frac{[\sigma(x)]^2}{Eh\Delta x}$$

where E = Young's modulus of coating, h = coating thickness and $\sigma(x)$ = stress in coating, determined mathematically from a knowledge of Poisson's ratio, Young's modulus, applied load and indenter radius. The work of adhesion is $W = \nu_1 + \nu_2 - \nu_{12}$ where ν_1 and ν_2 are surface energies of coating and substrate and ν_{12} is the interfacial energy. The criterion for adhesion is obtained by equating W for debonding Δx of interface to the stored elastic energy, i.e.

$$W = \frac{[\sigma(x)]^2}{2E}h$$

Various adhesion values, W, have been calculated for materials.

In their hardness prediction model, Burnett and Rickerby [21] developed a relationship between the film hardness and the composite and substrate hardness. This analytical model has been discussed in the section on modelling of thin-film hardness. An interface parameter χ was also defined in this model to be the factor by which the plastic zone radius changes due to effects of adhesion. The plastic zone is an area immediately around the indentor (see Fig. 4). In later work, Burnett and Rickerby [23, 36] related the parameter χ to the relative sizes of coating and substrate plastic zones, and postulated that for $\chi = 1$ poor film adhesion would result. This deduction was based on the reasoning that when $\chi = 1$, the relative radii of coating and substrate plastic zones would be equal, as opposed to cases where $\chi < 1$ or $\chi > 1$. Here, the film or the substrate deforming volumes are constrained by one another, resulting in better adhesion.

Furthermore, from the Burnett and Rickerby adhesion models, an interface stress is hypothesized to contribute to adhesion of films, and a low constraint interface stress thought to encourage the adhesion of coatings [36]. Based on the earlier hardness models [21, 22] a mathematical interpretation of adhesion assumes the driving force behind coating loss by adhesion as the sum of three components:

(i) an elastic–plastic indentation stress state similar to the hardness model,

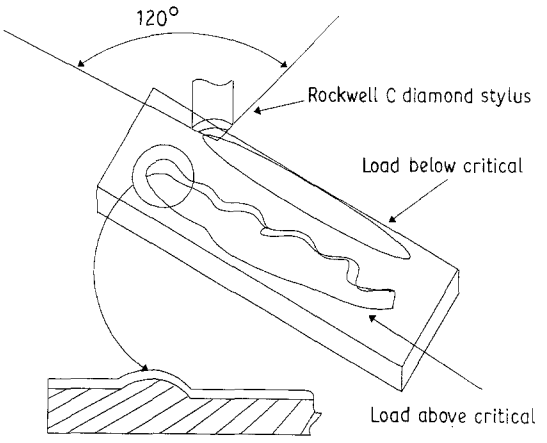

Figure 11 Schematic diagram of a scratch testing process (adapted from Perry [34]).

(ii) an internal stress component within the film, and

(iii) friction force [15].

These components are schematically shown in Fig. 12.

The stress components (i) and (ii) are relatively easily determined [21, 23]; however, estimation of the friction force component is difficult because of its dependence on applied load, the contact scale, and film substrate properties. Burnett and Rickerby [23] were able to provide mathematical relationships of the upper and lower bounds of the frictional forces. The frictional forces for a film on a soft substrate may be considered to be a line contact through the thickness of the coating, whereas for a coating with properties identical to those of the substrate the nature of the friction force can be approximated as a point contact. The nature of these forces are also shown schematically in Fig. 12.

These mathematical relationships were based on the coefficient of friction at the substrate–film interface, the applied normal load, the coating thickness, and the sliding direction angle. They showed that the magnitude of L_c which is dependent on the coating is also governed by the contributions of the frictional, indentation and internal energies during the scratch testing process. Thus, depending on the levels of these energies, L_c was shown to be directly or inversely propositional to the coating thickness. It is known that L_c is directly proportional to the coating thickness; however, Burnett and Rickerby [23] showed that an inverse relationship between L_c and coating thickness is also possible.

As mentioned above, the scratch test is widely used as an indicator of adhesion strength of TiN and other thin films. Burnett and Rickerby [36] have characterized various failure modes in scratch testing. Spalling and buckling failures of coatings occur as a result of compressive stress fields ahead of the moving stylus. Spalling results from complete delamination, while buckling is due to partial coating delamination at some distance ahead of the coating. This leads to cracking at the edge of the channel. In conformal cracking, semi-circular cracks occur within the scratch tracks only ahead of the indenter. Tensile cracking is

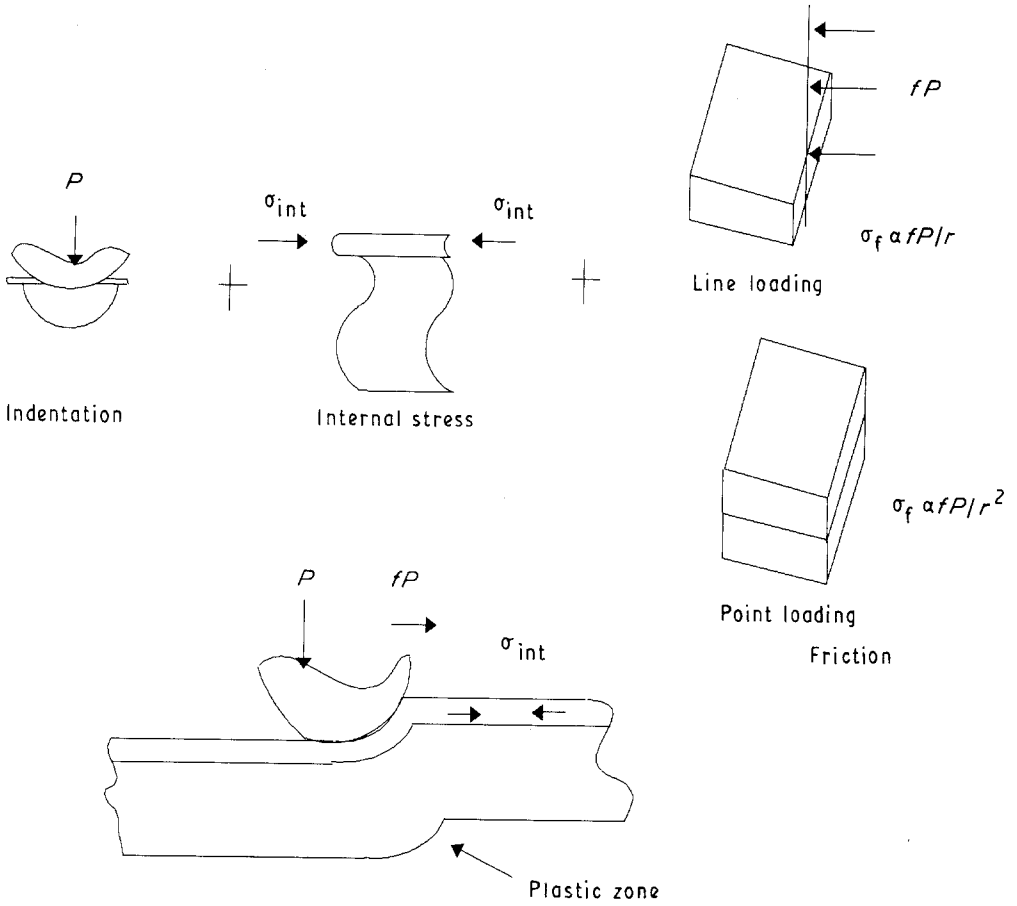

Figure 12 Elements of the scratch adhesion test (adapted from Burnett and Rickerby [23]).

similar to conformal cracking; however, the semi-circular cracks are behind the indenter. Fig. 13 shows schematically the various cracking modes.

According to researchers, a wide range of factors affect L_c values obtained from the scratch test. The most important of these are [36]: (i) coating thickness, (ii) hardness and Young's modulus of the substrate, (iii) hardness and Young's modulus of the coating, (iv) friction between the sliding stylus and the coated surface, and (v) internal stress in the coating. However, it is also not clear what failure criterion to consider when determining L_c values because coating failure may occur via spalling, buckling, chipping, conformal cracking and tensile cracking as mentioned above. Therefore, it has been suggested that L_c values be defined and quoted for the particular failure mode [36]. Experimentally, researchers [37] have also presented L_c data at two loads: (i) an upper load where the coating failed and (ii) a lower load which immediately precedes the test load.

Thus researchers believe that a clear understanding of the sources and existence of different stress fields is necessary to apportion the contributions of these fields and their effects on L_c for various substrate–film combinations. It is therefore important to further investigate the effect of friction on adhesion.

4.2. Experimental studies of thin-film adhesion

Perry [34, 38] studied the mode of coating loss of ion-plated TiN coatings deposited on stainless steel substrates. He observed that at loads below the critical load, the scratch channels were always smooth in appearance. At loads just below the critical load, local coating loss occurred at pre-existing fine cracks. Loss of coating was found to begin just ahead of the stylus. Additionally, the mode of coating loss depended on film thickness. For films less than 4 mm thick, local coating loss occurred at loads beyond L_c. For coating thickness between 4 and 6.5 mm, initial cracking of coating was observed perpendicular to the substrate surface at channel edge at loads below L_c. However, with increasing load the cracking extended across the scratch channel. For coatings thicker than 6.5 mm, extensive edge-cracking extending across channels was observed. The critical load was also found to be dependent on substrate material and coating thickness. A similar dependence of L_c on film thickness has been observed by Sproul [39].

An assessment of the variation of the adhesive strength with thickness indicates that with increasing coating thickness the bulk of the magnitude of shear stress is absorbed by regions close to the surface and shear stress is lower at the interface [40]. Thus, different modes of coating loss are observed at various thicknesses.

Adhesion studies of reactively sputtered TiN film on soft chromium steel substrates (Vickers hardness 176 H_V) reveal a thickness dependence of failure mode [41]. The thickness of the coating ranged from 0.7 to 4.0 μm, and at low loads for a 1.5 μm thick coating a smooth scratch channel was observed. As the load was increased, the coating started to crack perpendicular

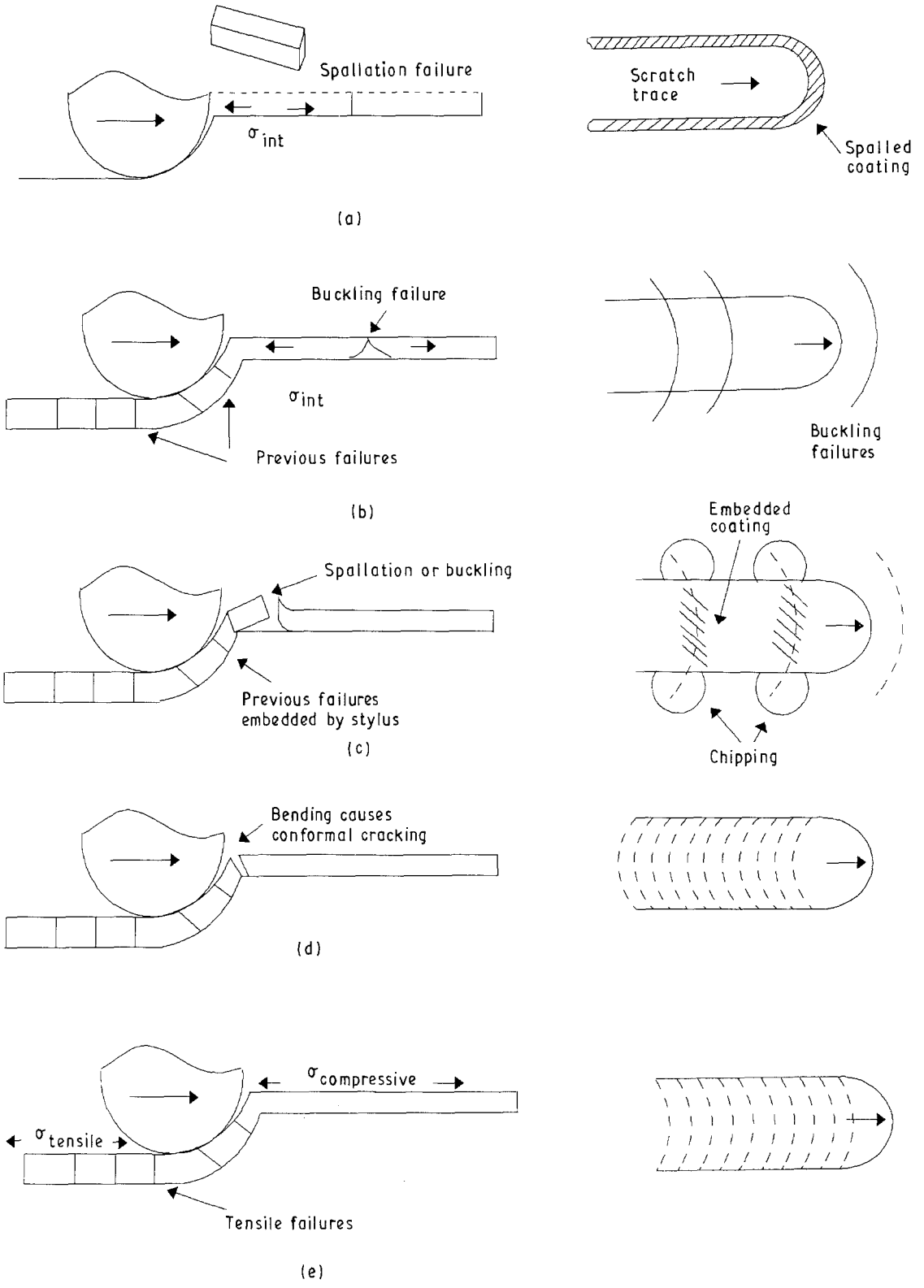

Figure 13 Schematic representation of coating failure modes in the scratch test in profile and plan views: (a) spalling failure, (b) buckling failure, (c) chipping failure, (d) conformal cracking, (e) tensile cracking (adapted from Burnett and Rickerby [22]).

to the substrate surface at the edge of the channel. This cracking behaviour was similar to that observed by Perry [34]. At high loads near L_c, the number of cracks increased and they were perpendicular to the stylus direction due to tensile stress near the edge of contact.

However, coating detachment from substrate was not evident because applied loads were lower than L_c. With increasing loads above L_c, cracks were formed perpendicular to the direction of the stylus with coating detachment. The same phenomenon of cracking perpendicular to stylus direction and coating detachment above L_c was observed for a 0.7 μm thick film. Although this study showed the coating crack mode to be independent of coating thickness in contrast to Perry's [34, 38] study, the coating failure mode observed in this study for reactively sputtered TiN on a soft substrate was different to that found for CVD or ion-plated TiN coatings examined by other researchers [34, 42]. This could be due to different

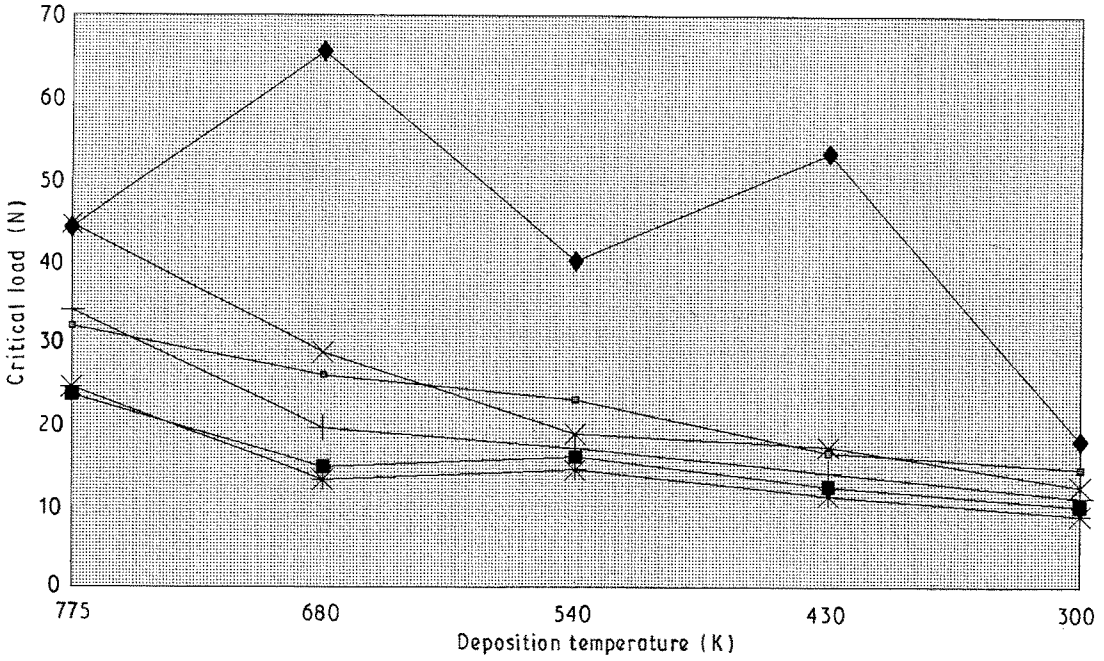

Figure 14 Variation of critical load with deposition temperature for high-speed steels: (■) M1, (+) M2, (*) M4, (□) M5, (*) M6, (◇) M7 (adapted from Kopacz and Jehn [46]).

substrate–film combinations, coating thicknesses, or processing parameters. Thus, a systematic examination is desirable to investigate the dependence of coating cracking due to adhesion on the parameters mentioned above.

The effect on L_c of the deposition temperature of TiN on various steels has revealed a peaking of L_c at a particular temperature [43, 44]. This effect is thought to be associated with microstructural changes occurring at various temperatures. A similar study by Al-Jaroudi *et al.* [45] examined the effect of substrate deposition temperature (200, 350 and 600 °C) on the interface chemical composition as well as the hardness and adhesion of magnetron-sputtered TiN on tool steel substrates. They observed peaking of the film hardness and L_c at 350 and 400 °C, respectively, and a decrease of the substrate hardness at the low deposition temperature of 200 °C. The substrate hardness decrease was explained by the formation of a softer annealed martensite from the original martensite. The hardness increase of the film was attributed either to diffusion of substrate material into the film or to changes in film microstructure at temperatures above 200 °C. Although the maximum critical load values agreed with the maximum in relative content of silicon, chromium and iron in the tool steel, no correlation has been established between the two and any intermediate phase formation. This aspect, therefore, needs to be studied.

Kopacz and Jehn [46], on the other hand, found a gradual decrease in critical load with decrease in deposition temperature for magnetron-sputtered TiN films. This is seen in Fig. 14 and may be due to insufficient mobility of the film-forming particles at lower temperatures, resulting in particle settlement at non-ideal substrate sites. Consequently, adhesion to the substrate is less. Therefore, it is evident from the above experimental studies that the interrelationships between deposition processes, deposition parameters, the evolved microstructures, and consequently film hardness and adhesion, are not completely known and thus deserve further investigation.

Similar microstructural effects on hardness have been observed by Valli *et al.* [47] who used the scratch test method to study the effect of nitrogen gas content on L_c for TiN films on stainless steel and HSS substrates. They observed a strong decrease of L_c with increasing nitrogen gas content and attributed this hardness phenomenon to the effect of incorporation of nitrogen in the film. L_c was also found to depend on the substrate type. With increasing load, the cracking of film progressed with semi-circular cracks ahead of indents due to stresses. Also, failure modes were found to be dependent on the local coating composition. Specifically, the Ti region exhibited failure by plastic deformation, a mixed phase of Ti and Ti_2N failed by cracking, whereas the TiN phase showed extensive cracking deformation. Although no microstructural correlations were made, it is believed that the phase composition differences in the coating may result in adhesion property differences because of variations in adhesion of the phases to substrates. This hypothesis is well supported by the work of Sundgren *et al.* [48–50] where it has been demonstrated that mechanical properties such as hardness of TiN films are dependent on processing parameters which largely control the composition of the coating and, therefore, the properties. In particular, these researchers observed different phases such as α-TiN, ε-TiN and δ-TiN at different N/Ti ratios which resulted in significant variations in film microhardness. This phenomenon was in turn found to be inherently linked to the partial pressures of the reactive gases.

Apart from scratch and adhesion tests, various other adhesion testing methods have been used by researchers [51, 52]. These include indentation, hammering, rolling, coining and metal stamping tests. Such tests are also able to characterize the various

coating failure modes such as cracking, flaking, chipping and wear.

Adhesion studies of single and multi-layer (TiC/TiCN/TiN) PVD and CVD TiN coatings on WC–Co substrates by scratch and indentation tests reveal that stylus conditions play a vital role in the scratch test, with L_c values being higher for better stylus conditions [53]. This is attributed to the creation of multiple cutting edges on used diamond tips, as compared to new ones, resulting in lower L_c values. It has also been observed that harder substrates had higher L_c values while the critical indentation load (P_{cr}) at cracking remained the same for all indentations [53]. From the adhesion studies, L_c values were observed to be insensitive to the coating thickness of ion-plated PVD films on carbide substrates in contrast to the work of Perry [34, 38] which exhibited a thickness dependence of the mode of coating loss and L_c of ion-plated TiN films on stainless steel substrates. With increasing load, the indentation interface crack length measurements yield a slope for the linear portion of the indentation load–lateral crack length function. This has been termed the interface fracture toughness parameter.

Cold-worked steel substrates, CVD-deposited with TiN, were subjected to scratch tests by Perry [42]. Microscopic examination of the scratch surface showed edge-cracking and semi-circular cracking within the channel with increasing loads. At further higher loads, complete stripping of coating occurred. Also, at higher loads of 5 kg and above, the microhardness of the channel was observed to be the same as that of the steel substrate, indicating no resistance of the coating to the stylus at these high loads. Acoustic emission measurements were also performed to confirm the onset of coating loss.

Hummer and Perry [36] conducted adhesion and hardness tests of ion-plated PVD TiN and TiC coatings on stainless steel, cold-worked steel and carbide substrates. They observed that below a certain critical thickness, substrate effects were imposed on hardness measurements. This can be likened to the indentation size effect. Coating removal in adhesion testing was by edge-flaking, cracking and channel coating loss. The mode of loss was also found to be dependent on the coating thickness. At low thicknesses, edge-flaking accompanied fine cracking, whereas with increasing thickness, semi-circular cracks occurred within channels associated with heavier edge-cracking. Since the critical load has been observed to be dependent on the coating thickness, the magnitude of shear stress evolved at the interface due to L_c may be responsible for the mode of coating loss. This mode is also affected by the elasticity of the substrate [37]. Thus the mode of coating loss may be controlled by the substrate type and surface roughness [54, 55], the coating thickness, and processing conditions. The nature and properties of the substrate affect adhesion and the nature of adhesion varies within a coating–substrate system [37].

The temperature dependence of PVD TiN adhesion has been observed for various metal substrate combinations. Page and Knight [26] observed a decline in

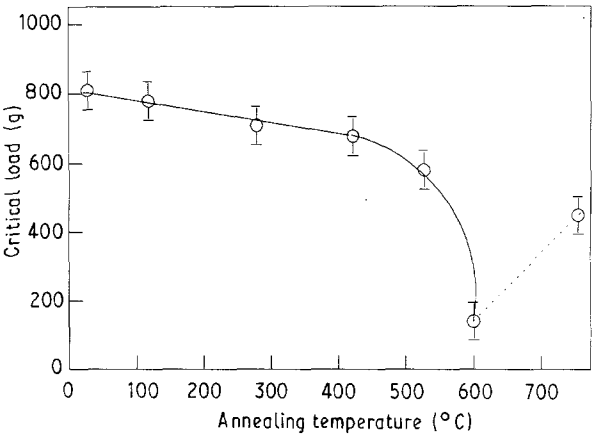

Figure 15 Variation of critical load with temperature (adapted from Page and Knight [26]).

L_c with increasing temperature (Fig. 15); they attributed this decline to increased porosity with temperature. Cheng *et al.* [56] deposited IP TiN on M50 steel with and without a Ti interlayer at various temperatures (100, 300 and 500 °C). It was observed that the adhesion values of film deposited at 100 and 500 °C with interlayers, and subsequently annealed, were highest. The suggested reason was a relocation of interfacial stresses by annealing and better chemical bonding. Similar improvements in adhesion of TiN coating to substrate by deposition of an interlayer has been observed by Rebenne *et al.* [57].

Thus, it is evident that substantial research has been done on the characterization of the adhesion property of TiN coatings deposited by various methods on various substrates. The adhesion failure modes – chipping, flaking, edge-cracking and coating channel loss – are known, as is the dependence of adhesion on coating thickness and substrate type. Semi-circular crack propagation within the channel has been observed with increasing coating loss. The condition of the indenting tip affects the value of L_c.

However, there does not exist any mathematical relationship between critical load, adhesion and material properties. It is necessary to study the role of friction in adhesion and the relationship between L_c values and the energy required to propagate a crack along the interface, i.e. the strength of adhesion [38]. Acoustic emission modelling of adhesive strength by formulation of the amount of energy required for coating–substrate separation and relating it to the generated signal may be a possibility. However, this requires knowledge of exact sources of separation of coating and substrate. The temperature dependence of hardness also needs to be quantified. This is important for metal cutting applications. Also, studies of the relationship between the shear modulus and adhesion and the effects of a Ti interlayer on adhesion would further enhance the understanding of the variables involved in promoting adhesion.

There is one important additional property of thin films – the internal stress. In the next section, the basic concepts of internal stresses in coating are examined and relevant literature reviewed.

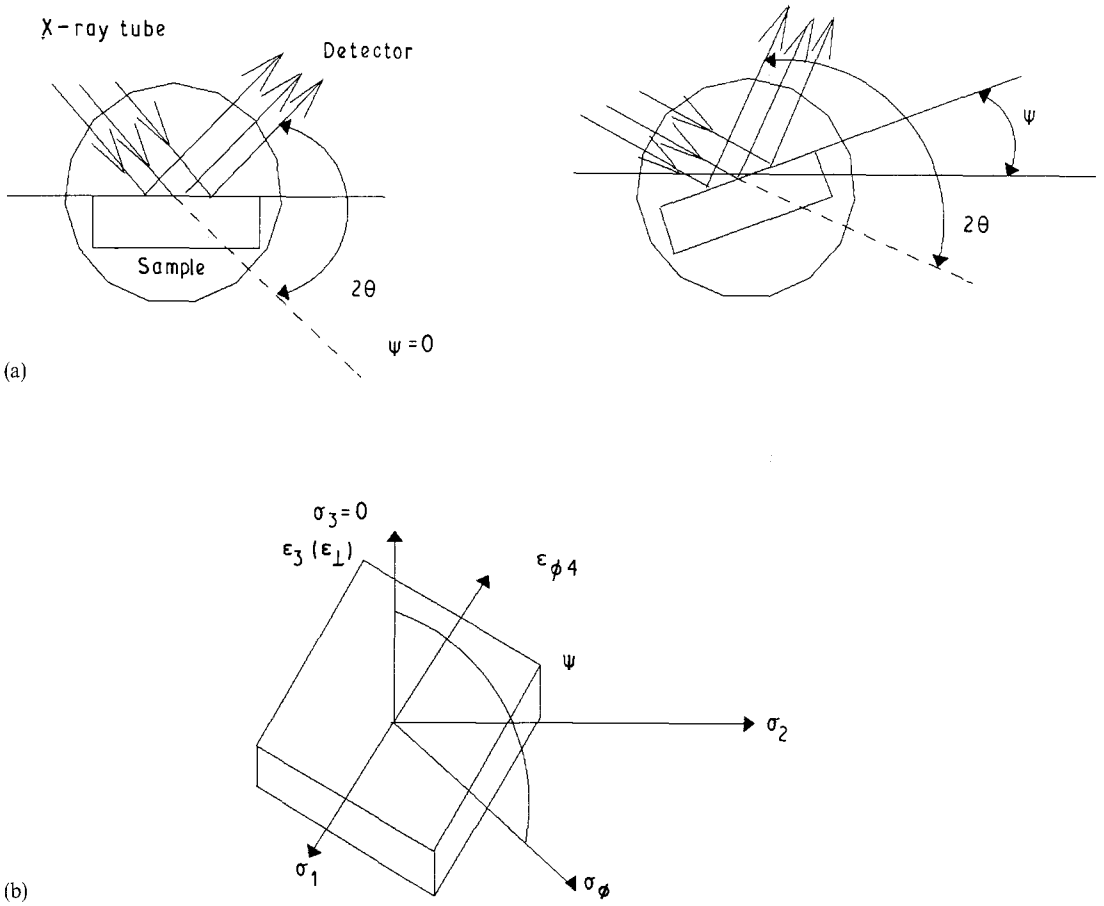

Figure 16 (a) Schematic representation of rotating an X-ray sample through an angle to allow families of planes, not parallel to the surface, to diffract; the case shown corresponds to an angle defined here as positive. (b) Definition of the stresses and angles used in the strain equation. (Adapted from Chollet and Perry [58].)

5. Residual stress in thin films

5.1. Theoretical modelling of thin-film stresses

The deposition process of thin films by CVD or PVD creates internal stresses within the film. The level of internal stress present in a coating affects its properties, particularly adhesion. The various deposition process parameters affect the internal stress of thin films in many ways. In the area of thin films, determination of the magnitude of internal stresses follows a simple principle.

As shown in Fig. 16, the stress in the plane of the coating is assumed to be two-dimensional [58] with σ_1 and σ_2 being the principal stresses. The normal stress σ_3 is assumed to be zero. The strain in the (ϕ, ψ) direction, $\varepsilon_{\phi\psi}$, is given as

$$\varepsilon_{\phi\psi} = \frac{d_\psi - d_0}{d_0} = \frac{a_\psi - a_0}{a_0}$$

where d_0 and a_0 are the unstressed lattice spacing and lattice parameter, respectively, and d_ψ and a_ψ correspond to those for the stressed condition in a plane perpendicular to the direction (ϕ, ψ). From elasticity theory

$$\varepsilon_{\phi\psi} = \frac{1 + \nu}{E}\sigma_\phi \sin^2\psi - \frac{\nu}{E}(\sigma_1 + \sigma_2)$$

for a Poisson's ratio ν, Young's modulus E and $\sigma_\phi = \sigma_1\cos^2\phi + \sigma_2\sin^2\phi$ in the surface of coating. From these two equations it can be deduced that a straight-line plot of $\varepsilon_{\phi\psi}$ as a function of $\sin^2\psi$ at constant ϕ has a slope related to σ, the stress, the elastic constants, and the lattice parameter in the stress-free condition:

$$\frac{a_\psi - a_0}{a_0} = \frac{1 + \nu}{E}\sigma_\phi \sin^2\psi - \frac{\nu}{E}(\sigma_1 + \sigma_2)$$

Thus the lattice parameter will be related to $\sin^2\psi$. This is the well known "$\sin^2\psi$" method (SSSP) for relating the lattice parameter, internal stresses and ψ [59].

X-ray diffraction methods are used for $\sin^2\psi$ measurements. Diffraction peaks for ψ and Θ (the Bragg angle) are located from which the lattice parameters are determined [59]. It is to be noted here that if stress gradients are present perpendicular to film surface, a curvature will be seen in the $\sin^2\psi$ plot. In addition, if shear stress gradients are present below the film surface, the $\sin^2\psi$ plot will separate into two branches for negative and positive values [58]. This is known as "ψ splitting".

The internal stresses in a film are believed to originate from two sources [60]. One, the thermal stress, is due to the differences in thermal expansion of film and substrate. The other, intrinsic stress, is due to the growth process or structural mismatch of film and substrate.

Rickerby [60] distinguished three types of lattice distortion due to stress effects in the sputter ion

plating (SIP) of TiN on steels. These lattice distortion types were

(i) macrostrains due to high internal stresses resulting from growth and thermal mismatch,

(ii) microstrains resulting from local fluctuation of lattice parameters due to point defects and dislocations, and

(iii) microstrains due to yield anisotropy between grains.

The macrostrain stress measurements can be done using the $\sin^2\psi$ plots described earlier. However, the microstrain measurements involve the determination of the broadening of X-ray diffraction peaks due to crystallite size broadening (β_c) and lattice strain (β_e) [60]. Here

$$\beta_c = \frac{K\lambda}{L\cos\Theta} \quad \text{and} \quad \beta_e = 4e\tan\Theta$$

where λ is the wavelength of the X-ray radiation, Θ is the Bragg angle, e the strain, and K is a shape factor for crystallites and is equal to unity. $1/L$ is the intercept following the equation of total broadening (β) obtained from the sum of β_c and β_e:

$$\frac{\beta\cos\Theta}{\lambda} = \frac{1}{L} + \frac{4e\tan\Theta}{\lambda}$$

Thus, microstrain measurements are possible from a plot of the above equation.

5.2. Experimental studies of thin-film stresses

Chollet and Perry [58] observed curvature (due to stress gradients perpendicular to the film surface) and splitting (due to the presence of shear stress below the coating surface) for CVD TiN films deposited on cemented carbides, and splitting only for IP TiN films on cemented carbides (Fig. 17). Stresses were found to be compressive in type in the plane of the coating for IP films; this is an effect of the PVD process itself due to a thermally induced stress redistribution in the substrate during the coating process. However, the stress value was slightly tensile for CVD TiN, which may also be attributed to the process itself releasing available strain energies at high deposition temperatures.

Rickerby [60] found anisotropic internal stress states and stress variation with substrate type for TiN films (Fig. 18). Stress gradients normal to the surface were tensile while stresses in the plane of the coating were compressive. It was also observed by Rickerby [60] that sputter ion plating produced lesser total internal stresses than in IP deposition as reported by Chollet and Perry [58], due to lower bias levels in SIP. Rickerby *et al.* [61] modelled residual internal stresses in tungsten and zirconia coatings. They observed the stress state in the film to be dependent on the material and coating thickness; Chollet and Perry [58] have also observed similarly. Macrostrain was found to increase with substrate bias for constant coating thickness and was maximum at the interface. Also observed was that deposition process parameters, particularly

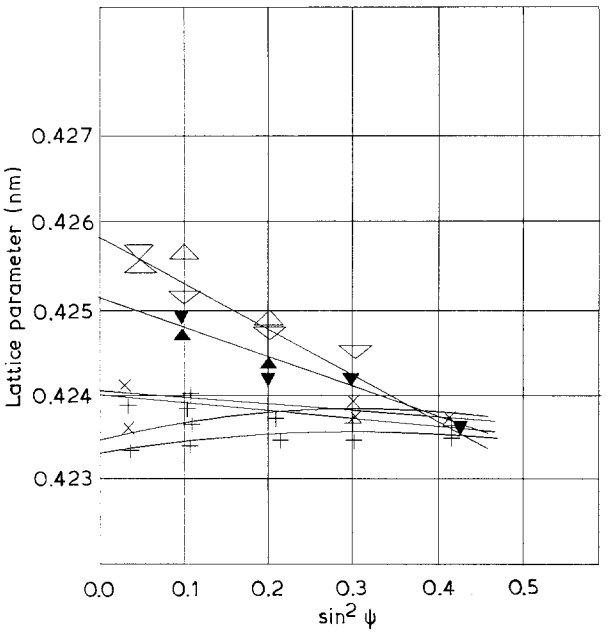

Figure 17 Variation in lattice parameter with $\sin^2\psi$ for TiN coated samples: ($\times$, $\triangle$, $\blacktriangle$) $\psi < 0$; ($+$, $\triangledown$, $\blacktriangledown$) $\psi > 0$ (adapted from Chollet and Perry [58]).

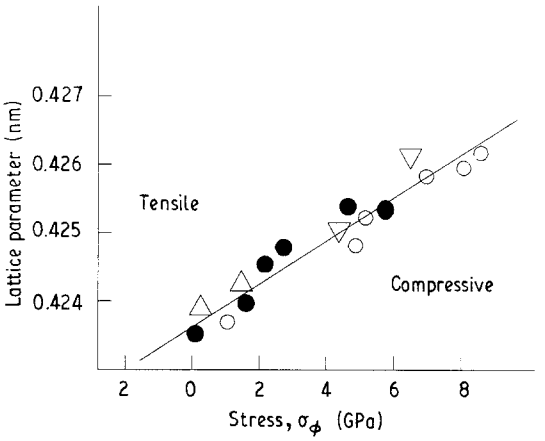

Figure 18 Variation of lattice parameter with internal stress for TiN coatings: (○) data of Rickerby [60]; ($\triangle$, ○, $\triangledown$) comparison data (adapted from [60]).

bias, affected the stress state and hardness of TiN films by affecting the growth process and microstructure.

Values of internal stresses exhibit variation with the X-ray type due to variation in the volume sampled resulting from differing penetration depths of the X-rays [61]. Curvature in the $\varepsilon_{\phi\psi}$ versus $\sin^2\psi$ plots is often noted, indicating the presence of stress gradients and shear stresses in films. Although compressive stresses are usually found in the plane of the film, tensile stresses may also be present. An example is the SIP deposition of TiN on stainless steel substrates [61]. Microstrain also varies with substrate type. TiN deposited on tool steel substrates exhibits a larger microstrain than when the substrate is removed. However, no microstrain is evident for TiN deposited on stainless steel [62].

Jindal *et al.* [53], noted the existence of compressive stresses in PVD TiN and attributed the cohesive coating failure to such stresses. The critical load (in scratch testing) was found to decrease with increasing

compressive stress due to the effect of stresses on cohesive coating failure.

As discussed before, X-ray diffraction methods are used to determine lattice parameters, lattice strain distribution and residual stress in different planes in TiN films. These parameters show large differences for different planes. For example, the lattice parameters of TiN films on cemented carbide for the (1 1 1) and (2 2 2) diffraction planes have yielded non-linear SSSP values [63]. ψ splitting has also been observed and great differences found in the levels of residual stresses in different lattice planes, with simultaneous existence of tensile and compressive residual stresses [60, 62, 63]. Such differences arise from different deposition methods and parameters, and dissimilar substrate types.

The effect of substrate type on coating is important from the standpoint of growth habits of deposits and levels of internal stresses in film. The factor regarding the level of mismatch between coefficients of thermal expansion of coating and substrate is also very important; the role of internal stress in determining the final coating microstructure has received little attention and should be investigated [64].

6. Effect of process parameters on coating properties

Target power, substrate bias and deposition rate have a significant effect on the properties of reactively sputtered TiN on cemented carbide inserts. For instance, Sproul *et al.* [65] measured an increase in Vickers microhardness from 970 to 3160 kg and in deposition rate from 100 to 480 nm min^{-1}.

Process parameters such as reactive gas partial pressure, substrate bias and composition significantly affect film properties [66, 67]. For example, the adhesion of coatings sputtered without bias is observed to be higher than that of bias-sputtered coatings [68]. Substrate bias and reactive gas partial pressure (gas composition) were varied by Sproul *et al.* [67] during high-rate sputtering of TiN on cemented carbide substrates to study the effect on hardness and adhesion. Substrate bias was varied between 0 and -200 V at constant gas pressure; gas partial pressure was varied between 0.025 and 0.20 mtorr at constant bias. It was observed that for bias levels between -80 and -200 V, the film hardness was greater than that of the bulk. This was ascribed to the effect of ion-bombardment on microstructure with bias resulting in hardness increases up to a certain bias; above this value hardness decreased due to damage of the film by ion bombardment. The N-Ti ratio had very little effect on hardness. This is in contrast to findings by Sundgren *et al.* [49]

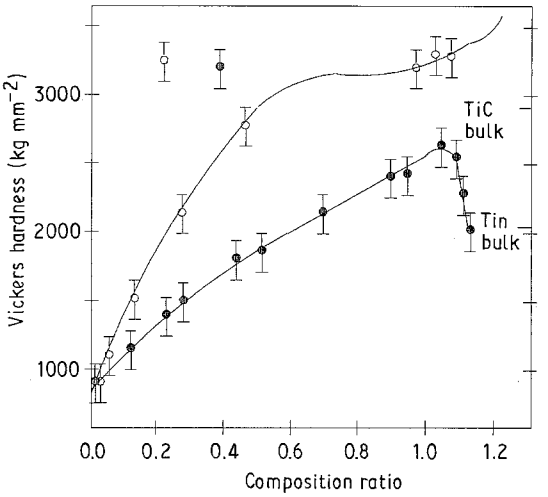

Figure 19 Vickers hardness as a function of reactive gas composition ratio (adapted from Sundgren *et al.* [49])

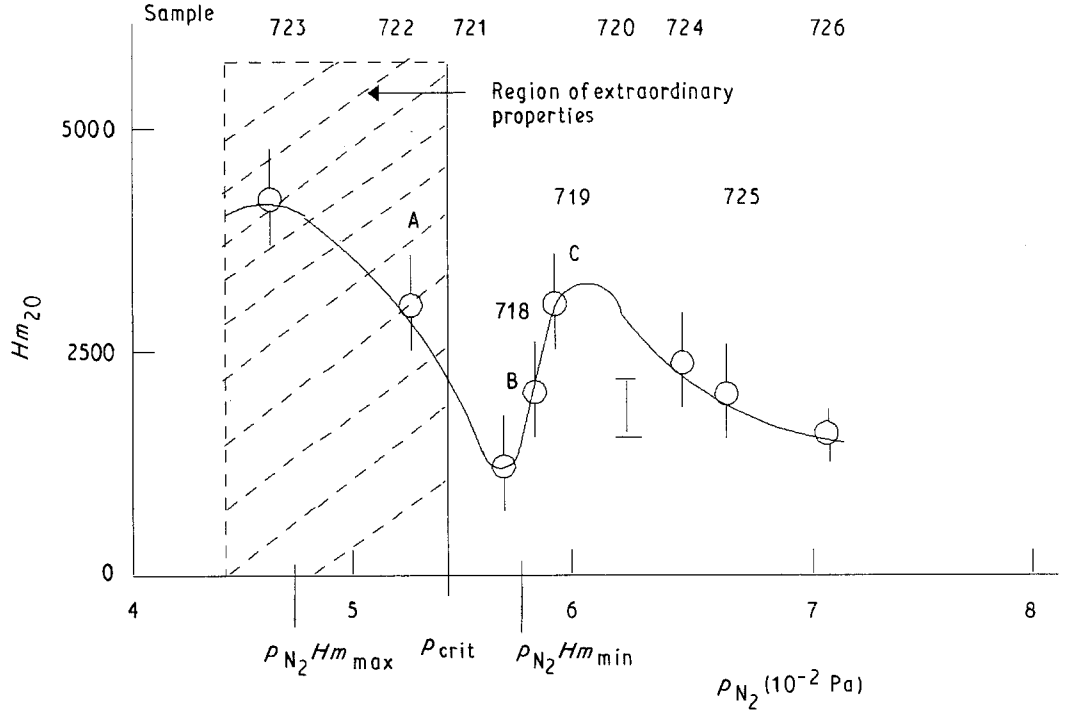

Figure 20 Microhardness for TN_x films as a function of nitrogen partial pressure (adapted from Musil *et al.* [69]).

(shown in Fig. 19) and Musil *et al.* [69] of the dependence of microhardness of TiN films on the reactive gas ratio partial pressure. According to the findings of Sundgren *et al.* [49], maximum film hardness is reached at stoichiometry. Musil *et al.* [69], however, observed the microhardness of TiN films to peak to a maximum at a particular gas partial pressure (Fig. 20). The difference could be due to differences in deposition process themselves – Sproul *et al.* [65] used substrate biasing unlike Musil *et al.* [69] and the gas partial pressure ranges were also different.

Deposition process and temperature affect the adhesion of films. This is evident in the work of Hilton *et al.* [70] and Rich and Woerner [71]. The former observed differences in adhesion due to different structures resulting at different deposition temperatures, while the latter found PVD coatings to be less resistant to spalling than their CVD counterparts due to coating morphological differences.

From the above review, it is evident that internal stresses are present in TiN films and their nature is governed by the deposition conditions. The measurement of stresses is done via X-ray diffraction (XRD) techniques. $\sin^2\psi$ plots indicate the presence or absence of shear stresses or stress gradients within the film. It seems that the creation of internal stresses within a film is a complex process whose magnitude or nature is dependent on the process [61]. Unlike hardness or adhesion modelling, stress modelling is yet to be rigorously developed although its measurement is fairly accurately possible. Also, as shown by Perry [72], lattice parameters determined by XRD techniques cannot be used as an indication of the residual stress because of splitting and curvature. Thus, the actual stress state may not correspond to a simple stress field in the plane of the film. Therefore, further investigations on modelling and quantification of the state of stress in TiN testing is warranted.

7. Corrosion, abrasion and erosion testing of TiN

As mentioned before, wear and corrosion resistance of TiN films are measured by subjecting the films to abrasive particles or a corrosive environment. Corrosion pits result from exposure of film to a corrosive atmosphere [73]. Defects in the coating structure, such as pinholes [74] and point defects [75], lead to wear by penetration of coating by the corroding agent. Thus, it is important to produce coatings with a dense structure.

The corrosion and abrasion resistance of CVD TiN on stainless steel by exposure to seawater and whirled sand, respectively, indicate that the lower the deposition temperature, the better the corrosion resistivity to sea water [76]. The Ni/Ti gas flow ratio also affects coating weight loss. In contrast, it has been seen that the abrasion resistance of films peaks at a particular deposition temperature; such effects are seen in Figs 21 and 22. The finer grain sizes and structure obtainable at lower deposition temperatures may contribute to lower corrosivity. Improved fracture toughness at low deposition temperatures may also be a reason for improved abrasion resistance of films.

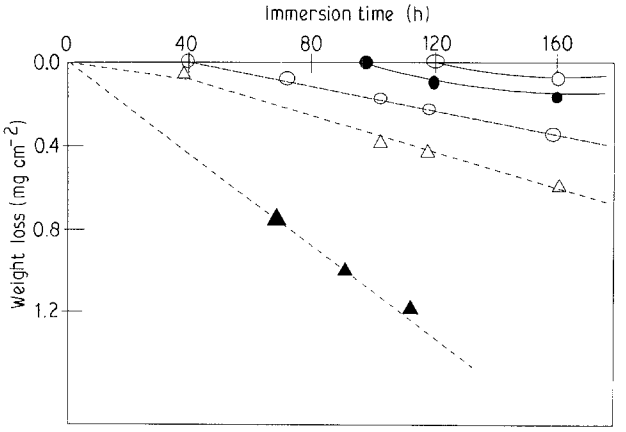

Figure 21 Weight loss with increasing immersion time in seawater for TiN-coated SUS 304 stainless steel with coating thickness (○) 0.9 μm and (●) 0.3–0.5 μm, and for various reference materials (deposition temperature, 950 °C): (△) nickel, (○) SUS 304 stainless steel, (▲) copper (adapted from Motojima and Kohno [76]).

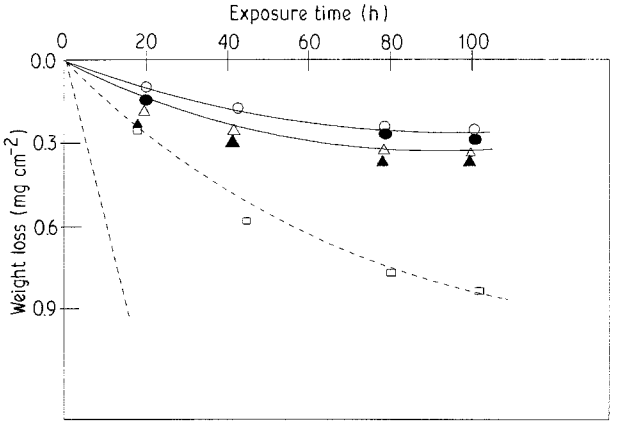

Figure 22 The weight loss with increasing exposure time in whirled sea-sand for (□) SUS 304 stainless steel and (- - -) copper, and TiN-coated SUS 304 stainless steel with coatings of various thicknesses (deposition temperature, 950 °C): (○) 1 μm, (●) 0.8 μm, (△) 0.5 μm, (▲) 0.3 μm (adapted from Motojima and Kohno [76]).

Jonsson *et al.* [77] proposed erosion as a parameter for testing the adhesion quality of TiN coatings. In their experiments, angular alumina was used as an erodent on TiN sputtered on HSS. Two types of study were performed. The first studied by SEM the craters formed by erosion, while the second quantified the coating removal for given particle doses, sizes, and velocities. Five types of crater were observed by SEM. These were

(i) craters less than 5 μm in size,
(ii) craters greater than 5 μm in size,
(iii) craters with cracks around the impression,
(iv) craters with coatings spalled around impressions, and
(v) deep craters with spalling.

The average surface area eroded was observed to be proportional to the erodent particle kinetic energy. The authors developed a mathematical model for the amount of film removal. The theoretical and experimental values of amount of film removal showed some differences. However, further studies are required to

determine the influence of film thickness and particle angle of incidence on erosion.

Coating thickness affects the mode and amount of abrasive and erosive loss. Thicker coatings have exhibited larger amounts of coating loss due to less dense outer regions in mild and severe abrasion and erosion of TiN films [78]. Microchipping is one observed mode of coating loss with severe abrasives. With mild abrasives, coating loss may occur by ploughing. The erosion loss of TiN coatings on carbon steel is seen to be dependent on the erodent angles of incidence. Thicker coatings are seen to offer more protection to alumina erosion and thinner coatings to glass bead erosion [78]. The failure modes are ploughing for thinner coatings and pitting, spalling and chipping for thicker ones.

The microstructure of a substrate also affects the tribological properties of films. For example, graphite nodules present in nodular iron act as detachment points for ion-plated TiN deposited on nodular cast iron [68]. Although a change in process parameters (for example, increase in reactive gas partial pressure and substrate bias) may improve tribological properties, such inherent microstructural properties profoundly affect the film properties [68].

8. Colour properties of TiN

One of the most striking property of a TiN coating is its pleasing golden colour. Thus, it is easy to understand its wide use for decorative purposes. Research indicates that the reflectance and colour properties are markedly dependent on the process type and parameter [79]. The usual method of relating reflectance and colour properties is through the determination of parameters L^*, a^* and b^* where L^* is the luminance, a^* is the value of redness and b^* is the value of yellowness as determined by a colorimeter [77].

Perry [80] observed a dependence on deposition rate of the colour of IP TiN deposited on stainless steel. With an increase of the deposition rate, the preferred orientation of TiN changed from (1 1 1) to a mixed (1 1 1)–(3 1 1) and colour became more yellow. With a (1 1 1) orientation the colour had a red cast which was attributed to increasing lattice distortion. Thus, it is feasible that changes in colour may be due to changes in texture and lattice spacing. The colour of TiN films is also influenced by ageing due to lattice contraction during storage [81]. Similar effects also occur on tempering of TiN films.

It has been postulated that changes in colour of ion-plated TiN films are not due to compositional changes, but due to orientation and lattice distortion [80]. However, Perry *et al.* [82] observed increases in reflectance of TiN films with increase in N/Ti ratio (Fig. 23). The redness and yellowness of films also increased with N_2 gas content. Samples produced at higher power settings exhibited an increase in redness. Tempering decreased the redness, and both a^* and b^* values for TiN increased with time. However, the correlation between tempering (due to lattic volume reduction) and colour change is not direct. Inverse relationships (decrease in yellowness) have also been

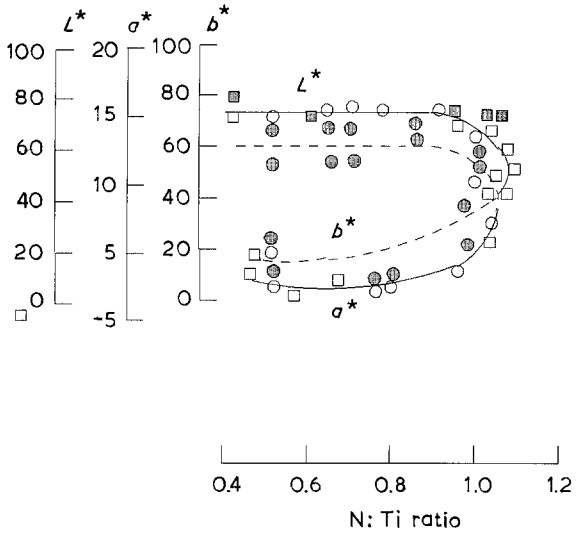

Figure 23 Variation with N: Ti ratio of colour coordinates of TiN films in as-received condition (open symbols) and when tempered (filled symbols) (adapted from Perry *et al.* [82]).

observed between tempering and colour [82]. Thus, there are yet unknown mechanisms that may contribute to changes in colour of TiN apart from process parameters and process types as above. Also, deviations from stoichiometry may have an effect on colour [83] as it has been found that an increase of partial pressure of nitrogen gas induces a change of TiN film colour from grey to gold [84], and oxygen incorporation in films alters the film reflectance.

9. Conclusions

A review of pertinent literature in theoretical and experimental research on the properties of TiN coatings suggests significant advances in modelling and the estimation of hardness, adhesion, strength, stress, corrosion and abrasion, and colour properties of these coatings. There is evidence of more work in certain areas (for example, adhesion and hardness modelling and measurement) than others (for example, colour). Based on this survey, future research should be directed at the following areas:

1. Modelling of hardness by the incorporation of the actual plastic zone morphology in the existing models.
2. Investigation of the diverse dependence of penetration resistance of TiN coatings at certain load ranges.
3. Development of a mathematical relationship between critical load, adhesion and material properties for TiN coatings.
4. Extensive investigation of the interrelationships between deposition processes, parameters, evolved microstructures and film properties.
5. Development of a model for stress prediction for TiN coatings.
6. Investigation of mechanisms leading to changes in colour properties of TiN coatings.

It is hoped that research efforts in the above areas will further clarify the relationships between the processing conditions, film–substrate combinations, evolved microstructure and film properties.

References

1. E. P. DeGARMO, J. T. BLACK and R. KOHSER, "Materials and Processes in Manufacturing", (Collier–Macmillan, 1989).
2. A. BHATTACHARYA, "Metal Cutting – Theory and Practice" (Central Book Publishers, Calcutta, 1984).
3. S. KALPAKJIAN, "Manufacturing Engineering and Technology", (Addison-Wesley, 1989).
4. S. CHATTERJEE, T. S. SUDARSHAN and S. CHANDRASHEKHAR, *J. Mater. Sci.* in press.
5. D. G. BHAT, in "Surface Modification Technologies" (Metallurgical Society, 1988) pp. 1–21.
6. R. F. BUNSHAH and H. C. RAGHURAM, *J. Vac. Sci. Technol.* **9** (1972) 1385.
7. A. J. ARONSON, D. CHEN and W. H. CLASS, *Thin Solid Films* **72** (1980) 535.
8. A. MUMTAZ and W. H. CLASS, J. Vac. Sci. Technol. **20** (1982) 345.
9. J. A. THORNTON, *Thin Solid Films* **107** (1983) 3.
10. W. D. SPROUL, *ibid.* **107** (1983) 141.
11. *Idem, J. Vac. Sci. Technol. A* **4** (1986) 2874.
12. P. D. FLOOD and P. J. WALSH, *Cutting Tool Engng* (Jan/Feb 1982) 4.
13. E. MOLL, R. BAHL, E. PULKER and E. BERGMAN, *Surf. Coatings Technol.* **39/40** (1989) 475.
14. H. RANDHAWA and P. G. JOHNSON, *ibid.* **31** (1987) 303.
15. D. A. HARDWICK, *Thin Solid Films* **154** (1987) 109.
16. E. TOROK, A. J. PERRY, L. CHOLLET and W. D. SPROUL, *ibid.* **153** (1987) 37.
17. P. J. BURNETT and D. S. RICKERBY, Coating Hardness, *Surf. Engng* **3** (1) (1987) 69.
18. M. E. O'HERN, R. H. PARRISH and W. C. OLIVER, *Thin Solid Films* **181** (1989) 357.
19. B. JONSSON and S. HOGMARK, *ibid.* **114** (1984) 257.
20. B. O. JOHANSSON, J. E. SUNDGREN, J. GREEN, A. ROCKETT and S. A. BARNETT, *J. Vac. Sci. Technol. A* **3** (1985) 303.
21. P. J. BURNETT and D. S. RICKERBY, *Thin Solid Films* **148** (1987) 41.
22. *Idem, ibid.* **148** (1987) 51.
23. *Idem, ibid.* **157** (1988) 233.
24. J. SUNDGREN and H. T. G. HENTZELL, *J. Vac. Sci. Technol. A* **4** (1985) 2259.
25. J. C. KNIGHT, T. F. PAGE and I. M. HUTCHINGS, *Thin Solid Films* **177** (1989) 117.
26. T. F. PAGE and J. G. KNIGHT, *Surf. Coatings Technol.* **39/40** (1989) 339.
27. D. T. QUINTO, G. J. WOLFE and P. C. JINDAL, *Thin Solid Films* **105** (1987) 19.
28. V. VALVODA, R. CERNY, R. KUZEL, J. MUSIL and V. POULEK, *ibid.* **158** (1988) 225.
29. V. VALVODA, R. KUZEL, R. CERNY, J. MUSIL, *ibid.* **156** (1988) 53.
30. J. MUSIL, S. KADLEC, J. VYSKOCIL and V. POULEK, *Surf. Coatings Technol.* **39/40** (1989) 301.
31. B. WENDLER, *Thin Solid Films* **141** (1986) 223.
32. V. VALVODA, R. CERNY, R. KUZEL, L. DOBIASOVA, J. MUSIL, V. POULEK and J. VYSKOCIL, *ibid.* **170** (1989) 201.
33. M. K. HIBBS, J. SUNDGREN, B. JACOBSON and B. O. JOHANSSON, *ibid.* **107** (1983) 149.
34. A. J. PERRY, *ibid.* **81** (1981) 357.
35. M. T. LAUGIER, *ibid.* **117** (1984) 243.
36. P. J. BURNETT and D. S. RICKERBY, *ibid.* **154** (1987) 403.
37. E. HUMMER and A. J. PERRY, *ibid.* **101** (1983) 243.
38. *Idem, ibid.* (1983) 167.
39. W. SPROUL, *ibid.* **107** (1983) 141.
40. D. J. RICH, A. J. PERRY and P. F. WOERNER, *ibid.* **154** (1987) 417.
41. J. H. JE, E. GYARMATI and A. NAOUMIDIS, *ibid.* **136** (1986) 57.
42. A. J. PERRY, *ibid.* **78** (1981) 77.
43. M. Y. AL-JAROUDI, H. T. G. HENTZELL and J. VALLI, *ibid.* **154** (1987) 425.
44. U. HELMERSSON, B. O. JOHANSSON, J. SUNDGREN, H. T. G. HENTZELL and P. BILLGREN, *J. Vac. Sci. Technol. A* **3** (1985) 308.
45. M. Y. AL-JAROUDI, H. T. G. HENTZELL, S. GONG and A. BENGTSON, Thin Solid Films **195** (1991) 63.
46. U. KOPACZ and H. A. JEHN, *Thin Solid Films* **126** (1985) 265.
47. J. VALLI, J. M. MOLARIUS and A. S. KORHONEN, *ibid.* **157** (1987) 351.
48. J. E. SUNDGREN, B. O. JOHANSSON and S. KARLSSON, *ibid.* **105** (1983) 353.
49. J. E. SUNDGREN, B. O. JOHANSSON, H. T. G. HENTZELL and S. E. KARLSSON, *ibid.* **105** (1983) 367.
50. J. E. SUNDGREN, B. O. JOHANSSON and S. KARLSSON, *ibid.* **105** (1983) 385.
51. T. ARAI, H. FUJITA and M. WATANABE, *ibid.* **154** (1987) 307.
52. P. HEDENQVIST, M. OLSSON and S. SODERBERG, *Surf. Engng* **5** (1989) 141.
53. P. C. JINDAL, D. T. QUINTO and G. J. WOLFE, *Thin Solid Films* **154** (1987) 361.
54. M. SALEHI, T. BELL and P. H. MORTON, paper presented at International Conference on Surface Modification Technologies, San Diego, 1991.
55. M. BENMALEK, P. GIMENEZ, J. P. PEYRE and C. TOURNIER, *ibid.*
56. C. C. CHENG, A. ERDEMIRE and G. R. FENSKE, *Surf. Coatings Technol.* **39/40** (1989) 365.
57. H. E. REBENNE, D. G. BHAT and P. F. WOERNER, in Proceedings of 3rd International Conference on Surface Modification Technologies, Neuchatel, Switzerland, August 1989, pp. 1–13.
58. L. CHOLLET and A. J. PERRY, *Thin Solid Films* **123** (1985) 223.
59. A. J. PERRY and L. CHOLLET, *J. Vac. Sci. Technol.* **4** (1986) 2801.
60. D. S. RICKERBY, *ibid.* **4** (1986) 2809.
61. D. S. RICKERBY, G. ECKOLD, K. T. SCOTT and I. M. BUCKLEY-GOLDER, *Thin Solid Films* **154** (1987) 125.
62. D. S. RICKERBY, A. M. JONES and B. A. BELLAMY, *Surf. Coatings Technol.* **37** (1989) 111.
63. A. J. PERRY, M. JAGNER, W. D. SPROUL and P. J. RUDNIK, *ibid.* **39/40** (1989) 387.
64. D. S. RICKERBY and S. J. BULL, *ibid.* **39/40** (1989) 315.
65. W. D. SPROUL, P. J. RUDNIK and M. GRAHAM, *ibid.* **39/40** (1989) 355.
66. D. S. RICKERBY and P. J. BURNETT, *Thin Solid Films* **157** (1988) 195.
67. W. D. SPROUL, P. J. RUDNIK and C. A. GOGOL, *ibid.* **171** (1989) 171.
68. K. H. KLOOS, E. BROSZEIT, H. M. GRABRIEL and H. J. SCHRODER, *ibid.* **96** (1982) 67.
69. J. MUSIL, L. BARDOS, A. RAJSKY, T. VYSKOCIL, B. DOLEZAL, G. LONCAR, K. DADOUREK and V. KUBICEK, *ibid.* **136** (1986) 229.
70. M. L. HILTON, G. J. VANDENTOP, M. SALMERON and G. A. SOMORJAI, *ibid.* **154** (1987) 377.
71. D. J. RICH and P. F. WOERNER, *J. Vac. Sci. Technol. A* **4** (1986) 2759.
72. A. J. PERRY, *Thin Solid Films* **170** (1989) 63.
73. P. J. MANTYLA, P. J. HELEVIRTA, T. T. LEPISTO and P. T. SIITONEN, *ibid.* **126** (1985) 275.
74. A. S. KORHONEN, J. M. MOLARIUS, E. HARJU and O. FORSEN, in "Surface Modification Technologies IV", edited by T. S. Sudharshan, D. G. Bhat and M. Jeandin (Minerals, Metals and Materials Society, 1991) pp. 311–316.
75. A. J. PERRY, *J. Vac. Sci. Technol. A* **6** (1988) 2140.
76. S. MOTOJIMA and M. KOHNO, *Thin Solid Films* **137** (1986) 59.
77. B. JONSSON, L. AKRE, S. JOHANSSON and S. HOGMARK, *ibid.* **137** (1986) 65.
78. D. S. RICKERBY and P. J. BURNETT, *Surf. Coatings Technol.* **33** (1987) 191.
79. A. MUMTAZ and W. H. CLASS, *J. Vac. Sci. Technol.* **20** (1982) 345.

80. A. J. PERRY, *Thin Solid Films* **135** (1986) 73.
81. *Idem, J. Vac. Sci. Technol. A* **4** (1986) 2670.
82. A. J. PERRY, M. GEORGSON and W. D. SPROUL, *Thin Solid Films* **157** (1988) 255.
83. A. J. PERRY, M. GEORGSON and C. G. RIBBING, *J. Vac. Sci. Technol. A* **4** (1986) 2674.
84. G. SCHILLER, G. BEISTER and W. SIEBER, *Thin Solid Films* **111** (1984) 259.

Received 26 March
and accepted 26 May 1992